PAPER

Energy spectrum and Landau levels in bilayer graphene with spin–orbit interaction

To cite this article: Francisco Mireles and John Schliemann 2012 *New J. Phys.* **14** 093026

New Journal of Physics
The open-access journal for physics

Energy spectrum and Landau levels in bilayer graphene with spin–orbit interaction

Francisco Mireles[1,2,3] **and John Schliemann**[1]

[1] Institut für Theoretische Physik, Universität Regensburg, D-93049 Regensburg, Germany

[2] Centro de Nanociencias y Nanotecnología, Universidad Nacional Autónoma de México, Ensenada, BC, CP 22800, Mexico

E-mail: fmireles@cnyn.unam.mx

New Journal of Physics **14** (2012) 093026 (24pp)
Received 6 March 2012
Published 14 September 2012
Online at http://www.njp.org/
doi:10.1088/1367-2630/14/9/093026

Abstract. We present a theoretical study of the band structure and Landau levels in bilayer graphene at low energies in the presence of a transverse magnetic field and Rashba spin–orbit interaction in the regime of negligible trigonal distortion. Within an effective low-energy approach the (Löwdin partitioning theory), we derive an effective Hamiltonian for bilayer graphene that incorporates the influence of the Zeeman effect, the Rashba spin–orbit interaction and, inclusively, the role of the intrinsic spin–orbit interaction on the same footing. Particular attention is paid to the energy spectrum and Landau levels. Our modeling unveils the strong influence of the Rashba coupling λ_R in the spin splitting of the electron and hole bands. Graphene bilayers with weak Rashba spin–orbit interaction show a spin splitting linear in momentum and proportional to λ_R, but scaling inversely proportional to the interlayer hopping energy γ_1. However, at robust spin–orbit coupling λ_R, the energy spectrum shows a strong warping behavior near the Dirac points. We find that the bias-induced gap in bilayer graphene decreases with increasing Rashba coupling, a behavior resembling a topological insulator transition. We further predict an unexpected asymmetric spin splitting and crossings of the Landau levels due to the interplay between the Rashba interaction and the external bias voltage. Our results are of relevance for interpreting magnetotransport and infrared cyclotron resonance measurements, including situations of comparatively weak spin–orbit coupling.

[3] Author to whom any correspondence should be addressed.

Contents

1. Introduction

Graphene and bilayer graphene (BLG) possess very distinctive physical properties [1, 2]. Neglecting interactions, the low-energy quasiparticles in pristine single- and double-layer graphene obey, respectively, linear and quadratic dispersion laws at the $K(K')$ symmetry points [3–5]. In the presence of a quantizing magnetic field $B > 0$, the relativistic massless Dirac fermions of graphene exhibit Landau levels (LLs) non-equidistant in energy, $E_n \propto \sqrt{|n|B}$, with $n = 0, \pm 1, \pm 2, \ldots$, the LL index [6]. The latter gives rise to the half integer quantum Hall effect at room temperature [7], and to the fractional quantum Hall effect at high magnetic fields in the presence of many-body effects [8, 9]. On the other hand, LLs for BLG show a rather intricate index sequence instead, with a roughly linear B-field dependence for low LLs and a $\sqrt{B}$ for high LLs [10–12]. At low energies, the LLs in unbiased BLG follow the sequence $E_n \propto \sqrt{|n|(|n|+1)}$ for $n \geqslant 1$ with a double degenerate zero-energy level, $E_0 = 0$ for $n = 0$ [13–15]. Experimentally, the LLs dipole-allowed transition energies in single-layer graphene and BLG have been studied in detail by cyclotron resonance [16–18]. Most recently, phonon-mediated inter-LL excitations were explored by magneto-Raman scattering experiments [19].

The particularly high interest in graphene spin physics is strongly motivated by the expected prospects of its use in nanoelectronics and spin-based devices for spintronics [20]. In this realm, the role of spin–orbit interaction (SOI) effects in graphene sheets is a topic under intense scrutiny. Two types of SOI in graphene have been identified: (i) the one induced by carbon intra-atomic SOI (*intrinsic*-SOI) and (ii) the SOI coming from the breaking of the space inversion symmetry of the hexagonal lattice (*extrinsic*-SOI); this is the so-called Rashba-SOI. The latter can have different origins, among which is the presence of a substrate, buckling, ad-atoms or external electric fields.

The magnitude of the excitation gap η of the *intrinsic*-SOI in a single layer is predicted to be very small (0.86–50 μeV) [21–27]. Likewise, estimates of the Rashba coupling λ_R lead to small values (a few tens of μeV) at typical electric fields ($\sim 0.16\,\mathrm{mV\,nm^{-1}}$) [23–25]. However, recent spin-resolved photoemission experiments in graphene/Au/Ni(111) showed enhancements of the Rashba coupling as large as 13 meV [28]. The induced distortions by neutral impurities (*ad-atoms*) [29, 30] and the interplay of buckling with Rashba-SOI also yield a significant enhancement of the spin splittings (up to 40 meV) [31]. The role of the impurities and lattice deformations seems to be crucial for the observed long spin relaxation times (up to 2 ns in BLG [32]) linked to SOI effects [33, 34], as well as for a non-monotonic dependence on bias voltage of the spin relaxation times in BLG due to the D'yakonov–Perel' spin-precession mechanism [35]. Large spin splittings (~ 0.22 eV) of the graphene π-states attributed to Rashba-SOI have been reported also in epitaxial graphene on a Ni substrate [36]. In theory, it has been shown that the Rashba-SOI can induce significant changes in the band structure of graphene [37, 38] as well as in BLG [39].

In graphene monolayers with Rashba coupling, the LLs are described by $E^{(1)}_{n,\mu\pm} = \mu\sqrt{\mathcal{E}^{(1)}_{n,\pm}}$, (in units of λ_R), with [37]

$$\mathcal{E}^{(1)}_{n,\pm} = (2n-1)\tilde{\Gamma}^2 + \tfrac{1}{2}\left(1 \pm \sqrt{1+4(2n-1)\tilde{\Gamma}^2+4\tilde{\Gamma}^4}\right) \tag{1}$$

for $n \geqslant 2$, where $\tilde{\Gamma} = \hbar v_F/l_B|\lambda_R|$, v_F is the Fermi velocity ($\sim 10^6\,\mathrm{m\,s^{-1}}$), $l_B = \sqrt{c\hbar/eB}$ is the magnetic length, $\hbar$ is Planck's constant over 2π, c is the light velocity in vacuum and $-e$ is the electron charge. Here $\mu = \pm$ stands for the electron/hole LL branch. The lowest $n = 0$ is given by $E_0 = 0$ while the $n = 1$ level gives rise to three modes: a zero mode $E^{(0)}_1 = 0$, in addition to two non-degenerate modes at $E_{1\mu} = \mu\sqrt{1+2\tilde{\Gamma}^2}$. Exact solutions for the LLs in monolayer graphene under the influence of a Zeeman field and SOIs have also been reported recently by De Martino *et al* [40].

In this paper, we show within low-energy effective theory that for biased BLG in which the Rashba effect is the dominant SOI, its LLs must follow $E^{(2)}_{n,\mu\pm} = \mu\sqrt{\mathcal{E}^{(2)}_{n,\pm}}$, with

$$\mathcal{E}^{(2)}_{n,\pm} = U^2 + \frac{n}{2}\left(\Gamma^2 + 2n\,\omega^2 \pm \sqrt{4\,\omega^4 + 4n\,\omega^2\Gamma^2 + \Gamma^4}\right) \tag{2}$$

for $n \geqslant 2$, with U the interlayer bias energy, $\Gamma = 2\sqrt{2}\lambda_R v_F\hbar/\gamma_1 l_B$ and $\omega = 2v_F^2\hbar^2/\gamma_1 l_B^2$, with γ_1 being the interlayer hopping energy. As occurs in graphene, in BLG with Rashba-SOI we obtain three modes for $n = 1$, namely the non-degenerate $E^{(2)}_{1\mu+} = \mu\sqrt{U^2+\Gamma^2+2\omega^2}$ and $E^{(2)}_{1-} = -U$, whereas for $n = 0$ its eigenvalue also vanishes in the absence of gating, $E^{(2)}_{0-} = U$. Equation (2) forms one of the main results of this paper.

The aim of this study was to investigate the energy spectrum and the LLs in BLG under the influence of sizable SOIs of both intrinsic and Rashba types. An effective low-energy Hamiltonian for BLG that includes both types of SOI and the Zeeman effect is derived within the Löwdin partitioning theory. Whereas the Rashba-SOI in single-layer graphene is known to modify its otherwise conic spectrum to a spectrum that includes two zero-gap bands and two gapped branches of width $2\lambda_R$ (with parabolic shape, similar to unbiased BLG) [37], here, in contrast, the (unbiased) BLG with Rashba-SOI shows a spin splitting that is linear in momentum and proportional to λ_R, but inversely proportional to the interlayer hopping parameter γ_1. We also predict a strong influence of the Rashba-SOI on the warping of the low-energy band

structure of biased bilayer at a comparatively weak spin–orbit coupling λ_R. It is found that the bias-induced gap in BLG decreases when the Rashba strength coupling is increased. It is further predicted that an unexpected asymmetric spin splitting of the LLs arises due to the interplay between the Rashba coupling and the external bias voltage.

The remainder of the paper is organized as follows. In section 2, we outline the model and derivation of the low-energy BLG effective Hamiltonian. The LL spectrum in the presence of Rashba-SOI is discussed in section 3. The band spectrum properties and the LLs of BLG with Rashba-SOI are analyzed in detail in sections 4 and 5. A summary of our results is given in section 6. Additionally, we provide three appendices. In appendix A we outline the derivation (the Löwdin partitioning theory) of the low-energy Hamiltonian in the presence of intrinsic and Rashba type SOIs, as well as the Zeeman effect. In appendix B, a detailed description of the eigenvalues of the low-energy Hamiltonian is given, and finally, in appendix C, the LLs for BLG with Rashba-SOI are derived.

2. Low-energy effective Hamiltonian for bilayer graphene (BLG)

Here we focus on the derivation of the low-energy effective Hamiltonian for BLG with SOI in the presence of magnetic field that eventually leads to equation (2). We start by considering a pile of two graphene layers (BLG) in which the sites A_2 of the upper layer 2 lie directly on top of the B_1 sites of the bottom layer 1 (AB-Bernal stacking). In the vicinity of the Dirac K symmetry point, the effective non-interacting BLG Hamiltonian H_0, written in terms of the spin-dependent basis $|\Psi_K^\dagger\rangle = \{\psi_{A_{1\uparrow}}, \psi_{A_{1\downarrow}}, \psi_{B_{1\uparrow}}, \psi_{B_{1\downarrow}}, \psi_{A_{2\uparrow}}, \psi_{A_{2\downarrow}}, \psi_{B_{2\uparrow}}, \psi_{B_{2\downarrow}}\}$, has the 8×8 matrix form

$$H_0 = \begin{pmatrix} H_+ & V_1 \\ V_1^\dagger & H_- \end{pmatrix}, \quad H_\pm = \begin{pmatrix} \pm U & 0 & \gamma\pi^\dagger & 0 \\ 0 & \pm U & 0 & \gamma\pi^\dagger \\ \gamma\pi & 0 & \pm U & 0 \\ 0 & \gamma\pi & 0 & \pm U \end{pmatrix}, \tag{3}$$

where $\pi = \pi_x + \mathrm{i}\,\pi_y$, $\boldsymbol{\pi} = \boldsymbol{p} + e\boldsymbol{A}/c = (\pi_x, \pi_y)$ is the canonical momentum, and $\boldsymbol{A}$ is the vector potential. Here $\gamma \equiv v_F = \gamma_0 a\sqrt{3}/2\hbar$, with $\gamma_0 \sim 3.1$ eV (intra-layer hopping energy) and $a = 0.246$ nm, is the lattice parameter [1]. The electrostatic potential $\pm U$ of the bottom/upper layer is gate voltage adjustable and opens a gap of $2U$ in the spectrum [2]. The dominant interlayer interaction in BLG is described to first approximation by the term

$$V_1 = \begin{pmatrix} -v_4\pi^\dagger & 0 & \gamma_1 & 0 \\ 0 & -v_4\pi^\dagger & 0 & \gamma_1 \\ v_3\pi & 0 & -v_4\pi^\dagger & 0 \\ 0 & v_3\pi & 0 & -v_4\pi^\dagger \end{pmatrix}, \tag{4}$$

where γ_1 is the nearest-neighbor (interlayer) hopping energy ($\sim 0.1\gamma_0$). The terms proportional to the velocities $v_3 = \gamma_3 a\sqrt{3}/2\hbar$ and $v_4 = \gamma_4 a\sqrt{3}/2\hbar$ arise due to second nearest-neighbor (interlayer) hopping processes associated with γ_3 and γ_4 tight-binding parameters, respectively [15, 41]. The former produces a trigonal warping whose characteristic energy is $E_3 = \frac{1}{2}m^* v_3^2 = \gamma_1(\gamma_3/2\gamma_0)^2 \sim 1$ meV, with $m^* = \gamma_1/2v_F^2$ being the electron effective mass [15], while the latter has a yet smaller characteristic energy, $E_4 = \frac{1}{2}m^* v_4^2 = \gamma_1(\gamma_4/2\gamma_0)^2 \sim 0.2$ meV. Since typically $E_{3,4} \ll \gamma_1$ in BLG, contributions in equation (4) coming from terms with velocities v_3 and v_4 are negligible. However, we should note that, when considering Rashba-SOI, there might be situations in which v_3 and v_4 may be important, particularly at very weak Rashba

strengths of the order of $E_{3,4}$. We would like to mention, nevertheless, that there is experimental (and theoretical) evidence of Rashba-SOI spin splittings of one order of magnitude [28, 29, 31] and even larger [36] than the typical distortion energies $E_{3,4}$. In any case, its inclusion in the model can be readily incorporated into the general derivation of the reduced effective Hamiltonian via the Löwdin perturbation theory described in appendix A. The regime in which there is a possible interplay among the $v_{3,4}$ terms and Rashba-SOI is beyond the scope of the present analytical study, and for the sake of clarity and simplicity these trigonal terms will be disregarded hereafter.

Taking into account explicitly the presence of *intrinsic-SOI*, Rashba-SOI and Zeeman splitting, the total eight-band effective Hamiltonian will read

$$H_K = H_0 + H_{\rm R} + H_{\rm I} + H_Z. \tag{5}$$

The second term to the right in equation (5) arises due to the influence of an effective electric field perpendicular to the BLG plane producing a Rashba type SOI. The leading contribution to the Rashba-SOI Hamiltonian, $H_{\rm R}$, is modeled as follows:

$$H_{\rm R} = \begin{pmatrix} 0 & {\rm i}\,\lambda_{\rm R}\,\sigma_- & 0 & 0 \\ -{\rm i}\,\lambda_{\rm R}\,\sigma_+ & 0 & 0 & 0 \\ 0 & 0 & 0 & {\rm i}\,\lambda_{\rm R}\,\sigma_- \\ 0 & 0 & -{\rm i}\,\lambda_{\rm R}\,\sigma_+ & 0 \end{pmatrix}, \tag{6}$$

where $\lambda_{\rm R}$ parameterizes the strength of the intra-layer Rashba-SOI, as in monolayer graphene, with $\sigma_\pm = \frac{1}{2}\left(\sigma_x \pm {\rm i}\,\sigma_y\right)$, with (σ_x, σ_y) being the usual 2×2 Pauli spin matrices. The intensity of the Rashba-SOI can be sizable ($\lambda_{\rm R} \sim 10\,{\rm meV}$) due, for instance, to the presence of a metallic substrate [28]. Within tight-binding theory, it is understood that the Rashba-SOI arises because of the effective nearest-neighbor hopping of two p_z orbitals with opposite spins under the presence of an applied transverse electric field [26].

Recently, it was predicted that $\lambda_{\rm R}$ can be even larger (of a few tens of meV) due to buckling effects in conjunction with external electric fields [31]. Furthermore, by varying the electric field, the Rashba parameter can be tuned. A possible inter-layer Rashba spin–orbit coupling of strength $\lambda_{\rm R}^{\perp}$ can, in principle, be present in BLG as well; however, such contributions will be ignored here because of its predicted weak influence on the energy bands for $\lambda_{\rm R}^{\perp}/\gamma_0 \lesssim 0.3$. [39]

Additionally, in the same basis set above, the *intrinsic*-SOI Hamiltonian for BLG (the third term on the rhs of equation (5)) shall follow the 4×4 matrix form

$$H_{\rm I} = \begin{pmatrix} \eta\, s_z & 0 & 0 & 0 \\ 0 & -\eta\, s_z & 0 & 0 \\ 0 & 0 & \eta\, s_z & 0 \\ 0 & 0 & 0 & -\eta\, s_z \end{pmatrix}, \tag{7}$$

with η the intrinsic SOI constant and s_z is the spin operator along the z-axis, perpendicular to the BLG plane. The intrinsic SOI is a second-order tunneling process (within tight-binding theory), which involves next-nearest-neighbor hopping events of p_z electrons of a given spin. As mentioned in the introduction, the value of the excitation energy η has been inferred to be very small in monolayer graphene at both $K\,(K')$ symmetry points ($\lesssim 50\,\mu{\rm eV}$) even if one considers interactions up to first order by including the unoccupied d and higher orbitals [25, 26]. Interestingly, in BLG, taking into account the interlayer overlapping of the π and σ bonds

yields enhanced values of the intrinsic-SOI: about one order of magnitude larger than in single-layer graphene ($\sim$0.1 meV) [42]. We would like to emphasize here that such values are still somewhat weak, compared with those relatively large strengths that reportedly the Rashba parameter λ_R can acquire (similar to the values attained in III–V semiconductors). Nevertheless, for generality, the intrinsic SOI has been incorporated into the present derivation of the low-energy effective Hamiltonian. This will be helpful when considering BLG in the extreme limit, i.e. when the intrinsic-SOI η is much stronger than the Rashba-SOI λ_R parameter ($\eta \gg \lambda_R$). However, we shall concentrate our discussion here on the band structure and LLs of BLG for the case $\lambda_R \gg \eta$; the opposite limit will be treated elsewhere.

The last term in equation (5) arises if an external magnetic field B is present, affecting the energetics of the quasiparticles in the form of a Zeeman interaction; H_Z, for a field perpendicular to the BLG plane, reads

$$H_Z = \Delta\,(\boldsymbol{I} \otimes \sigma_z), \tag{8}$$

where $\boldsymbol{I}$ is a 4×4 unit matrix, $2\Delta = g\,\mu_B B$ is the Zeeman splitting energy, g is the electron Landé factor and μ_B is the Bohr magneton. Note that even at relatively high magnetic fields ($B = 10$ T), the Zeeman splitting is still somewhat small ($\Delta \sim 1.1$ meV), while it is practically negligible at low fields. Note that the condition

$$\eta \lesssim \Delta \ll \lambda_R \lll \gamma_1 \tag{9}$$

typically holds at finite fields ($B \gtrsim 0.1$ T). This condition will allow us to work safely within the low-energy theory and derive an effective Hamiltonian for BLG, including the extrinsic (Rashba)-SOI, intrinsic-SOI and the Zeeman effect on the same footing. We should finally remark that the total Hamiltonian (5) is valid near the K symmetry point only. For the K' point of the Brillouin zone, the Hamiltonian $H_{K'} = \Sigma_y H_K \Sigma_y^{-1}$, with $\Sigma_y = \sigma_y \otimes \boldsymbol{I}$, should be used instead.

2.1. Low-energy bilayer Hamiltonian

Using the Löwdin partitioning theory [43, 44], the full 8×8 Hamiltonian H_K can be projected through a canonical transformation [45] into a 4×4 low-energy effective Hamiltonian $\mathcal{H}$ in an appropriate basis (see appendix A). The projected low-energy Hamiltonian can be further expressed in terms of Kronecker products of 2×2 matrices and conveniently separated into the sum of the Hamiltonians (keeping terms up to $1/\gamma_1^2$),

$$\mathcal{H} = \mathcal{H}^{(0)} + \mathcal{H}^{(1)} + \mathcal{H}^{(2)} + \mathcal{O}(1/\gamma^3), \tag{10}$$

in which the term independent of the interlayer hopping parameter γ_1 reads

$$\mathcal{H}^{(0)} = -\sigma_z \otimes (U\sigma_0 + \Delta\sigma_z) - \eta\,(\sigma_0 \otimes \sigma_z), \tag{11}$$

where σ_z is the z-component of the Pauli matrices and σ_0 is the 2×2 unit matrix. The dominant contribution to $\mathcal{H}$ is described by the Hamiltonian $\mathcal{H}^{(1)}$, given by

$$\mathcal{H}^{(1)} = -\frac{\gamma^2}{\gamma_1}\begin{pmatrix} 0 & (\pi^\dagger)^2 \\ \pi^2 & 0 \end{pmatrix} \otimes \sigma_x + \frac{2\mathrm{i}\,\lambda_R\gamma}{\gamma_1}\begin{pmatrix} 0 & -\pi^\dagger \\ \pi & 0 \end{pmatrix} \otimes s_+, \tag{12}$$

where we have defined the operator $s_\pm = \frac{1}{2}(\sigma_0 \pm \sigma_z)$. Without Rashba-SOI ($\lambda_R = 0$), equation (12) decouples to the usual effective BLG Hamiltonian obtained within low-energy theory in the absence of trigonal warping effects [13]. Such a term gives rise to the well-known

parabolic spectrum of the massive Dirac quasiparticles in BLG. The second term in $\mathcal{H}^{(1)}$ is linear in momentum and can be viewed as a renormalization of the Rashba coefficient due to the presence of the higher bands. Note that it scales as the inverse of the interlayer hopping energy γ_1.

The remaining terms proportional to $1/\gamma_1^2$ in equation (10) are compacted into the sum $\mathcal{H}^{(2)} = \sum_{i=1}^{4} h_i^{(2)}$, with

$$h_1^{(2)} = \frac{2U\gamma^2}{\gamma_1^2}\begin{pmatrix}\pi^\dagger\pi & 0\\ 0 & -\pi\pi^\dagger\end{pmatrix}\otimes\sigma_0,$$

$$h_2^{(2)} = \frac{U{\lambda_{\mathrm{R}}}^2}{\gamma_1^2}(\sigma_z\otimes s_+) + \frac{(\Delta+\eta)\lambda_{\mathrm{R}}^2}{\gamma_1^2}(\sigma_0\otimes s_+),$$

$$h_3^{(2)} = \frac{\mathrm{i}(2U+\Delta)\lambda_{\mathrm{R}}}{\gamma_1^2}\begin{pmatrix}\pi & 0\\ 0 & \pi^\dagger\end{pmatrix}\otimes\sigma_+ + \mathrm{h.c.},$$

$$h_4^{(2)} = -\frac{\mathrm{i}\Delta\lambda_{\mathrm{R}}}{\gamma_1^2}s_-\otimes\begin{pmatrix}0 & -\pi^\dagger\\ \pi & 0\end{pmatrix} + \frac{\mathrm{i}\,\eta\lambda_{\mathrm{R}}}{\gamma_1^2}s_+\otimes\begin{pmatrix}0 & \pi\\ -\pi^\dagger & 0\end{pmatrix}.$$

The low-energy effective Hamiltonian $\mathcal{H}$ described in equation (10) is valid within the energy range $\epsilon \lesssim \gamma_1$. Note that it will be fairly sufficient to keep only the leading order contribution $h_1^{(2)}$ in $\mathcal{H}^{(2)}$ given the typical smallness of the ratios $\lambda_{\mathrm{R}}^2/\gamma_1^2$, $\lambda_{\mathrm{R}}\Delta/\gamma_1^2$ and $\lambda_{\mathrm{R}}\,\eta/\gamma_1^2$ appearing in $\mathcal{H}^{(2)}$ together with the assumption $U < \gamma_1$. Hence the description of the low-energy (and momentum) effective Hamiltonian will be given by $\mathcal{H} = \mathcal{H}^{(0)} + \mathcal{H}^{(1)} + h_1^{(2)}$.

If we further neglect the Zeeman and the intrinsic SOI ($\Delta = \eta = 0$), the effective bilayer Hamiltonian with Rashba-SOI written in the atomic basis $\{\psi_{A_2\uparrow}, \psi_{A_2\downarrow}, \psi_{B_1\uparrow}, \psi_{B_1\downarrow}\}$ reduces to

$$\mathcal{H} = \begin{pmatrix} -U+\xi\pi^\dagger\pi & 0 & -\beta\,(\pi^\dagger)^2 & 0\\ 0 & -U+\xi\pi^\dagger\pi & -\mathrm{i}\,\alpha\,\pi^\dagger & -\beta\,(\pi^\dagger)^2\\ -\beta\,\pi^2 & \mathrm{i}\,\alpha\,\pi & U-\xi\pi\pi^\dagger & 0\\ 0 & -\beta\,\pi^2 & 0 & U-\xi\pi\pi^\dagger\end{pmatrix}, \tag{13}$$

where we have defined the parameters $\xi = 2U\tilde{\gamma}^2$, $\alpha = 2\tilde{\gamma}\,\lambda_{\mathrm{R}}$ and $\beta = \gamma_1\tilde{\gamma}^2$, with $\tilde{\gamma} = \gamma/\gamma_1$.

2.2. BLG spectrum with the Rashba effect at zero field

Without magnetic field ($B = 0$), $\pi^\dagger = \hbar k_- = \hbar(k_x - \mathrm{i}\,k_y)$ and $\pi = \hbar k_+ = \hbar(k_x + \mathrm{i}\,k_y)$ and the eigenvalues of equation (13) are readily determined by (appendix B)

$$\varepsilon_{\mu s}(k) = \frac{\mu}{2}\sqrt{4\,(U-\xi k^2)^2 + k^2\left(\sqrt{\alpha^2+4k^2\beta^2} - s\,\alpha\right)^2} \tag{14}$$

with $k = \sqrt{k_x^2+k_y^2}$. Here $\mu = \pm$ describe the electron/hole branch, while $s = \pm$ characterizes its spin chirality. Therefore, the low-energy spectrum consists of four spin-split bands, two conduction and two valence bands. For the unbias voltage case ($U = 0$), the spectrum reduces simply to

$$\varepsilon_{\mu s}^0(k) = \frac{\mu}{2}k\left(\sqrt{\alpha^2+4\beta^2k^2} - s\,\alpha\right). \tag{15}$$

We note that in contrast with single-layer graphene[4], in BLG the Rashba-SOI is induced by a linear spin splitting in the momentum of the conduction and valence bands, in close analogy with the Rashba interaction that arises in two-dimensional (2D) electron gases in semiconductor heterostructures. In addition, we observe that the cyclotron effective mass at the Fermi energy $m_{\rm c}^{(s)} = k/(\partial\, \varepsilon^0_{\mu s}/\partial\, k)$ turns out to be spin dependent as long as $\lambda_{\rm R} \neq 0$ following the relation

$$m_{\rm c}^{(s)} = m^* \frac{4\mu\sqrt{\pi n}\lambda_\beta \sqrt{1+4\pi n\lambda_\beta^2}}{1+8\pi n\lambda_\beta^2 - s\sqrt{1+4\pi n\lambda_\beta^2}}, \tag{16}$$

with $\lambda_\beta = \beta/\alpha = \gamma/2\lambda_{\rm R}$, and we have expressed the Fermi wave number in terms of the 2D carrier density via $k_{\rm F} = \sqrt{\pi n}$. Note that in the limit case $\lambda_\beta \to \infty$, the cyclotron mass $m_{\rm c}^{(s)} \to \mu m^* = \mu\gamma_1/2v_{\rm F}^2$, as one expects for unbiased BLG in the absence of SOI. However, as the carrier density $n \to 0$, the cyclotron effective mass does not diverge as predicted by tight-binding models.

The normalized eigenvectors $|\psi_{ks}^{(\mu)}\rangle$ of $\mathcal{H}$ corresponding to the electron and hole bands $\mu = \pm$, respectively, for the case of spin up ($s = +$) are written in the four-vector form (appendix B)

$$|\psi_{k+}^{(\mu)}\rangle = \frac{1}{\sqrt{1+(\chi_+^{(\mu)})^2}} \begin{pmatrix} -{\rm i}\,{\rm e}^{-2{\rm i}\phi}\sin(\theta/2)\chi_+^{(\mu)} \\ {\rm e}^{-{\rm i}\phi}\cos(\theta/2)\chi_+^{(\mu)} \\ -{\rm i}\cos(\theta/2) \\ {\rm i}\,{\rm e}^{-{\rm i}\phi}\sin(\theta/2) \end{pmatrix}, \tag{17}$$

while the normalized eigenvectors for the spin down ($s = -$) electron/hole bands are specified by

$$|\psi_{k-}^{(\mu)}\rangle = \frac{1}{\sqrt{1+(\chi_-^{(\mu)})^2}} \begin{pmatrix} {\rm i}\,{\rm e}^{-2{\rm i}\phi}\cos(\theta/2)\chi_-^{(\mu)} \\ {\rm e}^{-{\rm i}\phi}\sin(\theta/2)\chi_-^{(\mu)} \\ {\rm i}\sin(\theta/2) \\ {\rm i}\,{\rm e}^{-{\rm i}\phi}\cos(\theta/2) \end{pmatrix}, \tag{18}$$

in which we have defined the dimensionless parameter

$$\chi_s^{(\mu)} = \frac{U - \xi k^2 + \mu\sqrt{\mathcal{R}_{\mu s}^2 + (U-\xi k^2)^2}}{\mathcal{R}_{\mu s}}, \tag{19}$$

with $\theta = \tan^{-1}(2\beta k/\alpha)$, and ϕ is the azimuthal angle of the in-plane wave vector, $\boldsymbol{k} = k(\cos\phi, \sin\phi)$. The denominator of equation (19) is explicitly $\mathcal{R}_{\mu s} = \mu\, \varepsilon^0_{\mu s}(k) = |\varepsilon^0_{\mu s}(k)|$, which implies that $\mathcal{R}_{+s} = \mathcal{R}_{-s}$ and therefore the relation $\chi_\sigma^{(+)}\chi_\sigma^{(-)} = -1$ is always satisfied. Without external bias voltage ($U = 0$), the parameter $\chi_\sigma^{(\pm)}$ reduces to ± 1 for all k.

2.2.1. Spin and valley polarization. The expectation values of the valley (charge) polarization and spin orientation are defined as $\langle\boldsymbol{\tau}\rangle_{\mu s} = \langle\psi_{ks}^{(\mu)}|\boldsymbol{\tau}|\psi_{ks}^{(\mu)}\rangle$ and $\langle\boldsymbol{S}\rangle_{\mu s} = \langle\psi_{ks}^{(\mu)}|\boldsymbol{S}|\psi_{ks}^{(\mu)}\rangle$, respectively. Here the valley and spin operators are $\boldsymbol{\tau} = \boldsymbol{\sigma}\otimes\sigma_0$ and $\boldsymbol{S} = \frac{\hbar}{2}(\sigma_0\otimes\boldsymbol{\sigma})$, with

[4] The spectrum in single-layer graphene with Rashba coupling is described by two zero-gap bands and two gapped bands split by $2\lambda_{\rm R}$ [37].

$\boldsymbol{\sigma} = (\sigma_x, \sigma_y, \sigma_z)$ being the vector of Pauli matrices. Using the results of equations (17) and (18) the components for the charge polarization lead to the expressions

$$\langle \tau_x \rangle_{\mu s} = \frac{2\chi_s^{(\mu)}}{(\chi_s^{(\mu)})^2 + 1} \sin\theta \cos(2\phi), \tag{20}$$

$$\langle \tau_y \rangle_{\mu s} = \frac{2\chi_s^{(\mu)}}{(\chi_s^{(\mu)})^2 + 1} \sin\theta \sin(2\phi), \tag{21}$$

$$\langle \tau_z \rangle_{\mu s} = \frac{(\chi_s^{(\mu)})^2 - 1}{(\chi_s^{(\mu)})^2 + 1}, \tag{22}$$

whereas the components of the spin polarization (in units of $\hbar/2$) satisfy

$$\langle S_x \rangle_{\mu s} = -s \sin\theta \sin(\phi), \tag{23}$$

$$\langle S_y \rangle_{\mu s} = +s \sin\theta \cos(\phi), \tag{24}$$

$$\langle S_z \rangle_{\mu s} = s \frac{1 - (\chi_s^{(\mu)})^2}{1 + (\chi_s^{(\mu)})^2} \cos\theta. \tag{25}$$

As occurs with the standard Rashba-SOI in semiconductors, in BLG the orientation of the spin polarization in the plane is always perpendicular to the direction of the momentum, $\langle \boldsymbol{S} \rangle \cdot \boldsymbol{k} = 0$. We note also that, in contrast with single-layer graphene, in BLG the dot product $\langle \boldsymbol{S} \rangle \cdot \boldsymbol{\tau} \neq 0$ in general. Interestingly, as long as there is a bias voltage present ($U \neq 0$), both the spin and valley polarizations have a non-zero component out of the BLG plane (along the z-axis). However, in the absence of bias voltage ($U = 0$) the amplitude of the charge and spin polarization develops k-dependent oscillations. Explicitly, $|\langle \boldsymbol{\tau} \rangle| = |\langle \boldsymbol{S} \rangle| = \sin\theta$ for all $|\boldsymbol{k}| \neq 0$, and vanishes at $\boldsymbol{k} = 0$, in close analogy with the known result in single-layer graphene [46]. From equations (22)–(24) the spin polarization in the unbiased configuration can be compactly written as

$$\langle \boldsymbol{S} \rangle_{\mu s} = \frac{2\, s\beta}{\sqrt{\alpha^2 + 4\beta^2 k^2}} (\hat{z} \times \boldsymbol{k}); \tag{26}$$

that is, $\langle \boldsymbol{S} \rangle_{\mu s}$ is forced to lie in the BLG plane. Clearly, as the Rashba-SOI coefficient $\lambda_R \to 0$, i.e. $\alpha \to 0$, the magnitude of spin polarization reaches its maximum value, $|\langle \boldsymbol{S} \rangle_{\mu s}| \to 1$, as the electron/hole spin is conserved. Finally, we note that equation (26) for the spin orientation in unbiased BLG is formally identical to that obtained in single-layer graphene with Rashba-SOI [37].

3. Landau levels (LLs) in BLG with Rashba spin–orbit interaction (SOI)

For a magnetic field $B \neq 0$ perpendicular to the BLG plane, the operators π and $\pi^\dagger$ do not commute any longer since its components fail to do so, and of course, care has to be exercised in their ordering. By making the substitution into equation (13) of the momentum operators in terms of the Bose operators, $\pi^\dagger = \sqrt{2}\hbar\, a^\dagger / l_B$ and $\pi = \sqrt{2}\hbar\, a / l_B$ with $\left[a, a^\dagger\right] = 1$, the effective Hamiltonian in the limit of low bias ($U \ll \gamma_1$) takes the form

$$\hat{H}_L = -\begin{pmatrix} U & 0 & \omega\,(a)^2 & 0 \\ 0 & U & \mathrm{i}\,\Gamma a & \omega\,(a)^2 \\ \omega\,(a^\dagger)^2 & -\mathrm{i}\,\Gamma a^\dagger & -U & 0 \\ 0 & \omega\,(a^\dagger)^2 & 0 & -U \end{pmatrix} \tag{27}$$

with the notation $\Gamma = \sqrt{2}\hbar\,\alpha/l_B$ and $\omega = 2\hbar^2\beta/l_B^2$. The eigenfunctions of $\hat{H}_L$ can now be written in the form $|\psi_n\rangle = (c_1^{(n-2)}|n-2\rangle, c_2^{(n-1)}|n-1\rangle, c_3^{(n)}|n\rangle, c_4^{(n+1)}|n+1\rangle)^T$, where $|n\rangle \equiv \xi_n$ are the usual harmonic oscillator eigenfunctions satisfying $a^\dagger|n\rangle = \sqrt{n+1}|n+1\rangle$ and $a|n\rangle = \sqrt{n}|n-1\rangle$. Consequently, one can write the expectation value $\langle\psi_n|\hat{H}_L|\psi_n\rangle = \langle\phi_n|\mathcal{H}_n|\phi_n\rangle$, with

$$\mathcal{H}_n = \begin{pmatrix} -U\sigma_0 & \mathcal{F}_n \\ \mathcal{F}_n^\dagger & U\sigma_0 \end{pmatrix}, \tag{28}$$

and $|\phi_n\rangle = (c_1^{(n-2)}, c_2^{(n-1)}, c_3^{(n)}, c_4^{(n+1)})^T$ satisfying the normalization condition $\langle\phi_n|\phi_n\rangle = 1$, while

$$\mathcal{F}_n = -\begin{pmatrix} \omega\sqrt{n(n-1)} & 0 \\ i\,\Gamma\sqrt{n} & \omega\sqrt{n(n+1)} \end{pmatrix}. \tag{29}$$

The eigenvalues of (28) lead to the Landau spectrum given by equation (2), which, in the absence of a bias gate voltage across the layers ($U = 0$), reads (appendix C)

$$\varepsilon^0_{n,\mu\pm} = \frac{\mu}{\sqrt{2}}\sqrt{n\Gamma^2 + 2n^2\omega^2 \pm n\sqrt{4\omega^4 + 4n\omega^2\Gamma^2 + \Gamma^4}}, \tag{30}$$

for $n \geqslant 2$. In order to gain further physical insight into the behavior of the LLs in BLG, it is illustrative to analyze the limit cases at zero, weak (large) Rashba-SOI relative to the magnetic field strength, with and without bias voltage.

3.1. Approximate solutions for $U = 0$

(i) *Zero Rashba-SOI* ($\Gamma = 0$). In the vanishing Rashba-SOI strength limit, equation (30) reduces to $\varepsilon^0_{n,\mu\pm} = \mu\sqrt{n(n\pm1)}\,\omega_0 B$, with $\omega_0 = e\hbar/m^*c$, and coincides with the LL spectrum (double degenerate in spin) reported in the literature for BLG in the absence of Rashba-SOI. The linear response with B stems from the parabolic dispersion laws of BLG for this case.

(ii) *Weak Rashba-SOI* ($\Gamma/\omega \ll 1$). At very weak Rashba-SOI strengths (large fields), the LLs still evolve approximately linear with B, but shifted by a small energy proportional to λ_R^2, described by

$$\varepsilon^0_{n,\mu\pm} \simeq \mu\left(\omega_0 B \pm \frac{\Gamma_0^2}{4\omega_0}\right)\sqrt{n(n\pm1)}, \quad \mu = \pm \tag{31}$$

with $\Gamma_0 = \sqrt{2\omega_0/m^*}(\lambda_R/v_F)$ and $n \geqslant 2$. Since $\Gamma_0^2/4\omega_0 = \lambda_R^2/\gamma_1$, only rather large Rashba-SOI coefficient ($\lambda_R \simeq \gamma_1$) strengths give rise to significant broken degeneracies of the electron/hole LLs as described next in the opposite regime.

(iii) *Strong Rashba-SOI* ($\Gamma/\omega \gg 1$). Alternatively, in the very strong Rashba-SOI limit (small fields), the LL level spectrum is well described by $\varepsilon^0_{n,\mu+} \simeq \mu\sqrt{n}\,\Gamma = \mu\,\Gamma_0\sqrt{nB}$ and $\varepsilon^0_{n,\mu-} \simeq \mu(\omega_0^2/\Gamma_0)\sqrt{n(n^2-1)}B^{3/2}$, with $n \geqslant 2$. The change in the field dependence from $B^{1/2}$ for the $\nu = +$ chiral states to $B^{3/2}$ for the $\nu = -$ states is unique in BLG and gives rise to a multiplicity of LL crossings as shown later.

In addition, the energy spectra with LL level index $n = 1$ and 0 are special cases giving rise to three levels, one at zero energy ($\epsilon_{0-} = 0$) and two non-degenerate levels for $n = 1$. In the high-field limit $\Gamma/\lambda_R \gg 1$, we obtain $E_{1\mu+} \simeq \mu\sqrt{2}(\Gamma_0^2/4\omega_0 + \omega_0 B)$, while we obtain $E_{1\mu-} \simeq \mu\Gamma_0\sqrt{B}$ in the weak field regime.

3.2. Approximate solutions for $U \neq 0$

(i) *Zero Rashba-SOI in the $\omega \ll U$ limit*. In this case the quantum states should follow

$$\varepsilon_{n,\mu\pm} \simeq \mu U + \frac{\mu}{2U} n(n \pm 1)\, \omega_0^2 B^2; \tag{32}$$

clearly, in addition to the aperture of an energy gap of $2U$ between the spin-degenerate electrons/hole LLs, the presence of the gate voltage induces a deviation from the linear dependence on B occurring at $U = 0$, to a parabolic behavior with B instead. This is also a known result in the literature [11, 12].

(ii) *Weak Rashba-SOI in the regime $U \gg \omega \gg \Gamma$*. Here the LLs still behave quadratic in B but with a spin-dependent shift linear in B given as

$$\varepsilon_{n,\mu\pm} \simeq \mu U + \frac{\mu\, n(n \pm 1)}{2U} \left(\omega_0^2 B^2 \pm \frac{\Gamma_0^2 B}{2} \right), \tag{33}$$

the term proportional to Γ_0^2 is responsible for the anticrossings of the fan spectrum of the $\nu = \pm$ states.

(iii) *Strong Rashba-SOI in the regime $U \gg \Gamma \gg \omega$*. In contrast with the case of $U = 0$, at very large Rashba-SOI strengths the LL spectrum follows (to leading order) linear behavior with B for the positive chirality states ($\nu = +$), whereas for the negative ($\nu = -$) quantum states it develops a cubic dependence instead. Explicitly, they are given by

$$\varepsilon_{n,\mu+} \simeq \mu U + \frac{\mu\, \Gamma_0^2}{2U} nB, \quad \varepsilon_{n,\mu-} \simeq \mu U + \frac{\mu\, \omega_0^4}{2U\Gamma_0^2} n(n^2 - 1) B^3. \tag{34}$$

Such a drastic change in the field dependence of the LLs with different spin chirality states ($\nu = \pm$) will dramatically enhance the degree of their spin splitting and the multiplicity of the level crossing as studied in the next section.

All of these discussed above hold true for $n > 2$. The cases $n = 0, 1$ are treated separately as in the condition for $U = 0$. In the limit $U \gg \omega \gg \Gamma$ (small Rashba-SOI or large fields) $\varepsilon_{1\mu+} \simeq \mu(U + \omega_0^2 B^2/U)$ and $\varepsilon_{1\mu+} \simeq \mu(U + \Gamma_0^2 B/U)$ for the large Rashba-SOI (or small Rashba-SOI) case ($U \gg \Gamma \gg \omega$), while $\varepsilon_{1-} = -U$ for both regimes. The case for zero LL index is $\varepsilon_{0-} = U$, which also holds in both regimes.

3.3. Spin polarization of the LLs

The eigenfunctions of equation (28) for the nth LL of a given electron (hole) band μ in biased BLG are given in appendix C. From equations (C.18) and the orthogonality of the oscillator wave functions ξ_n, it follows that the valley $\langle \boldsymbol{\tau}^{(n)} \rangle_{\mu\nu}$ and $\langle \boldsymbol{S}^{(n)} \rangle_{\mu\nu}$ spin polarization lying in the plane of BLG vanishes identically for all LLs. General expressions for the valley and spin polarization are provided in equations (C.19) and (C.20). We note that the valley polarization in the perpendicular direction turns out to be k independent and that, for the unbiased case, it vanishes for all LLs. Furthermore, the zth component of the spin polarization of the nth LL with $U = 0$ reduces to

$$\begin{aligned} \langle S_z^{(n)} \rangle_{\mu\nu} &= -\frac{\nu}{2} (\cos\vartheta_{n-} + \cos\vartheta_{n+}) \\ &= -\frac{2\nu\, \omega^2}{\sqrt{4\omega^2 + 4n\, \omega^2 \Gamma^2 + \Gamma^4}}, \end{aligned} \tag{35}$$

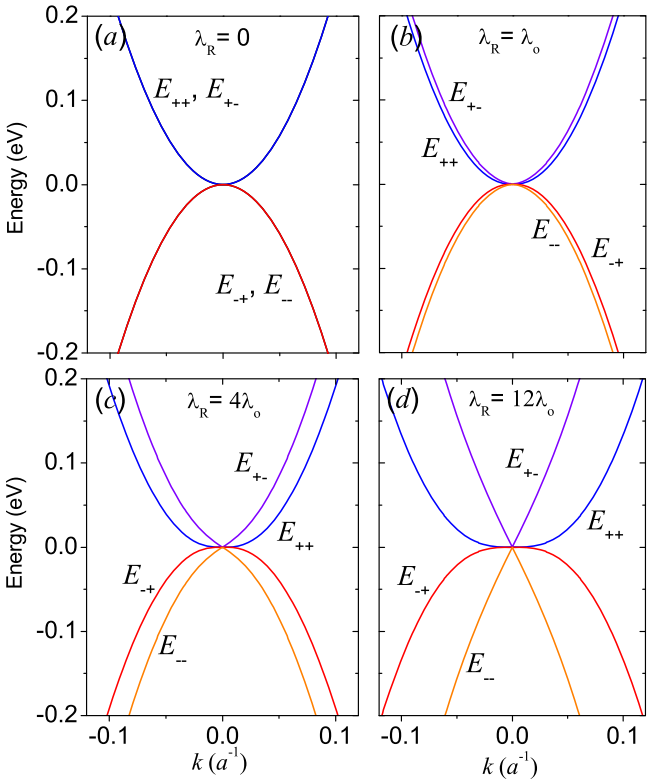

Figure 1. Low quasiparticle energy spectrum for BLG with Rashba-SOI. The spin degeneracy of the bands at $\lambda_R = 0$ (a) is lifted for $\lambda_R \neq 0$ (b)–(d). When the strength of the Rashba parameter is increased, the symmetry of the bands is broken, producing a cone shape for the innermost bands ($s = -$) at high values of λ_R.

where, as before, $\nu = \pm$ denotes the plus/minus n-LL of a given $\mu = \pm$ electron/hole branch. In the limit of a high field $\langle S_z^{(n)} \rangle_{\mu\pm} \to \mp 1$, full polarization is reached, and the state $\nu = \pm$ coincides with the spin magnetization signs ($\mp$) of the LLs. If the limit $B \to 0$ is taken, then the spin polarization $\langle S_z^{(n)} \rangle_{\mu\pm} \to \pm 2(\omega_0^2/\Gamma_0^2)B$.

4. Band structure properties in bilayer graphene with Rashba-SOI

The low-quasiparticle-energy band structure for unbiased BLG with Rashba-SOI, as predicted by equation (15) at zero field, is illustrated in figure 1 for different values of λ_R strength. In the absence of Rashba-SOI ($\lambda_R = 0$) the well-recognized parabolic spin-degenerate conduction and valence bands touching at its extrema at $k = 0$ are depicted in figure 1(a). For non-zero λ_R the spin degeneracy of the bands is broken, inducing a k-linear spin splitting of width $\Delta_s(k) = |E_{\pm,\mp} - E_{\pm,\pm}| = \alpha k$. For relatively weak Rashba-SOI ($4\beta^2 k^2 \gg \alpha^2$) the band dispersion follows a parabolic behavior, $\varepsilon^0_{\mu s}(k) \simeq \mu(\beta^2 k^2 - \frac{1}{2}(s)\alpha k)$, as shown in figure 1(b). On the other hand, if the condition $4\beta^2 k^2 \ll \alpha^2$ holds, then the relation (15) evolves to a linear spectrum for the inner bands ($\varepsilon^0_{\mu s}(k) \simeq \mu\alpha k$ for $s = -$) and to a k-cubic spectrum for the outermost bands ($\varepsilon^0_{\mu s}(k) \simeq \mu\beta^2 k^3/\alpha$ for $s = +$) as plotted in figure 1(d). Similar drastic changes

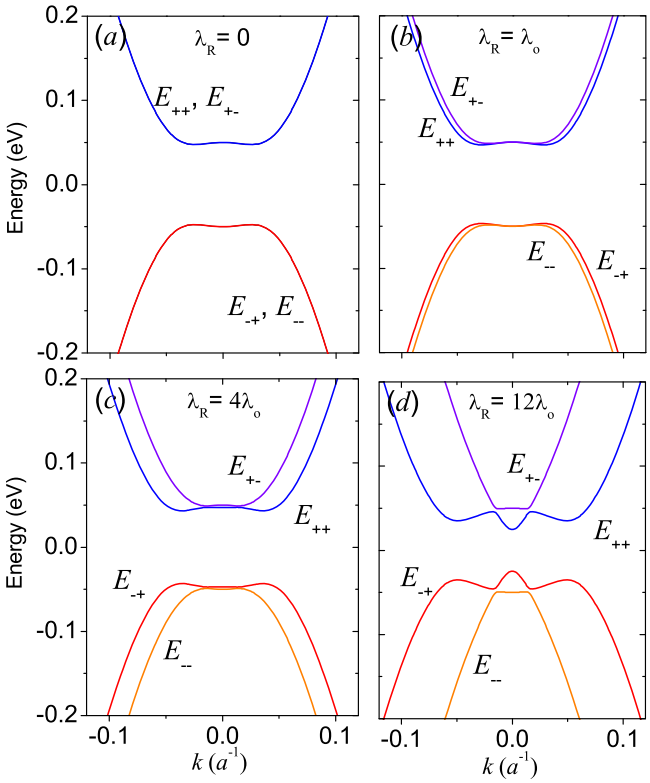

Figure 2. Low-energy spectrum for biased BLG with Rashba-SOI. Here $U = 0.050\,\text{eV}$. The bias voltage-induced gap decreases as the Rashba parameter λ_R increases.

in the band structure due to large Rashba-SOI strengths were reported earlier numerically by van Gelderen and Morais Smith [39] within a tight-binding framework; see, for instance, the low-energy bands near the Dirac points in figure 1(d) of that reference.

In the intermediate regime (figure 1(c)), the innermost bands interpolate from k-linear behavior for electron/hole momentum very close to the Dirac point, to k-cubic dependence for high momentum. In contrast, the $s = +$ bands seem to be well described by the cubic spectrum for all values of k. Such remarkable asymmetric behavior of the spectrum of BLG with Rashba-SOI is certainly unique, since it is not seen in monolayer graphene, nor in semiconductors with the Rashba-type SOI. These peculiar characteristics of the spectrum of BLG would have interesting consequences for the electronic and spin-transport properties.

In figure 2, we show the BLG low-energy spectrum for finite bias voltage ($U = 0.050\,\text{eV}$) at various Rashba coupling strengths ($\lambda_R = 0$, λ_0, $4\lambda_0$ and $12\lambda_0$). As in the unbiased case, without Rashba-SOI, the bands are spin degenerate (figure 2(a)). A gap of $2|U|$ at $k = 0$ is opened between the conduction and valence bands turning BLG into a semiconductor. Moreover, a band-bending appears at small wave numbers (low momentum) due to the interplay with the bias gate voltage U. This is the so-called 'Mexican-hat-like' shape of the lowest energy bands well reported in the literature. From equation (14), in this regime ($\lambda_R = 0$) and $ka \lesssim 1$ the bands are reasonably well described by $\varepsilon_{\mu s}(k) \simeq \mu(U - \xi k^2 + (\beta^2/2U)k^4)$. For non-zero λ_R (figures 2(b)–(d)) the spin degeneracy is lifted. When the Rashba-SOI parameter increases the

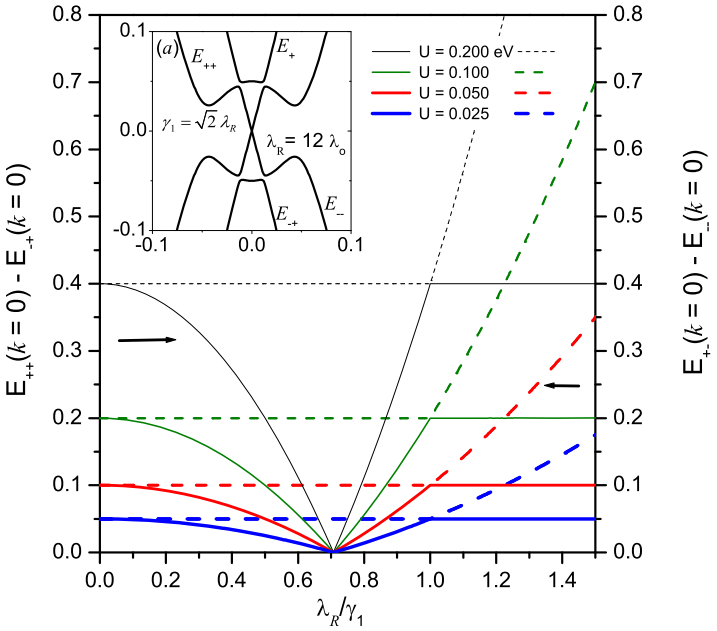

Figure 3. The Rashba-SOI effectively modulates the gap size of the biased BLG. Inset (a) shows the spectrum of the bands for the critical Rashba-SOI parameter that ensures a closing gap, $\lambda_R = \gamma_1/\sqrt{2}$ with $U = 0.025\,\text{eV}$, $\gamma_1 = 0.22\,\text{eV}$ and $\lambda_R = 12\lambda_0$.

lowest/highest conduction/valence bands become more warped and the gap tends to decrease as the lowest conduction band E_{++} evolves from a Mexican-hat-like shape to an inverted one, and vice versa for the highest valence band E_{-+}, see figure 3(d) calculated using equation (A.14). The behavior of the gaps $\Delta_{g+} = E_{++} - E_{-+}$ (for the innermost bands) and $\Delta_{g-} = E_{+-} - E_{--}$ (for the outermost bands) as a function of the ratio λ_R/γ_1 is plotted in figure 3 for different bias voltages U. The gap Δ_{g+} in BLG closes as the Rashba parameter increases, reaching its minimum (zero gap) at $\lambda_R = \gamma_1/\sqrt{2}$, to then gradually and linearly open again as λ_R/γ_1 is increased up to 1. For $\lambda_R/\gamma_1 > 1$ the gap Δ_{g+} remains constant. Inset (a) of figure 3 shows the band structure for biased BLG with $U = 0.025\,\text{eV}$ illustrating the zero-gap condition. Analogous behavior can be seen in the numerical plot depicted in figure 7(b) of [39]. Note that our analytical low effective modeling for the BLG band structure allows us to also capture the anomalous behavior of the lowest bands (near the Dirac points) under finite bias and relatively large Rashba coupling. In addition, it predicts that the closing of the gap occurs provided that $\lambda_R = \gamma_1/\sqrt{2}$, regardless of the magnitude of the bias voltage applied.

5. LL spectrum in BLG with Rashba-SOI

The LL energy spectrum as a function of magnetic field (up to 12 T) for BLG with Rashba-SOI according to equation (2) is plotted (from $n = 0$ to 41) in figures 4 and 5 for the unbiased and biased cases, respectively. The zero gate voltage ($U = 0$) and without Rashba-SOI case shows an LL fan diagram that is linear with B and degenerate in spin (figure 4(a)), as expected, because of the parabolic behavior of the energy bands and since there is no spin-dependent mechanism

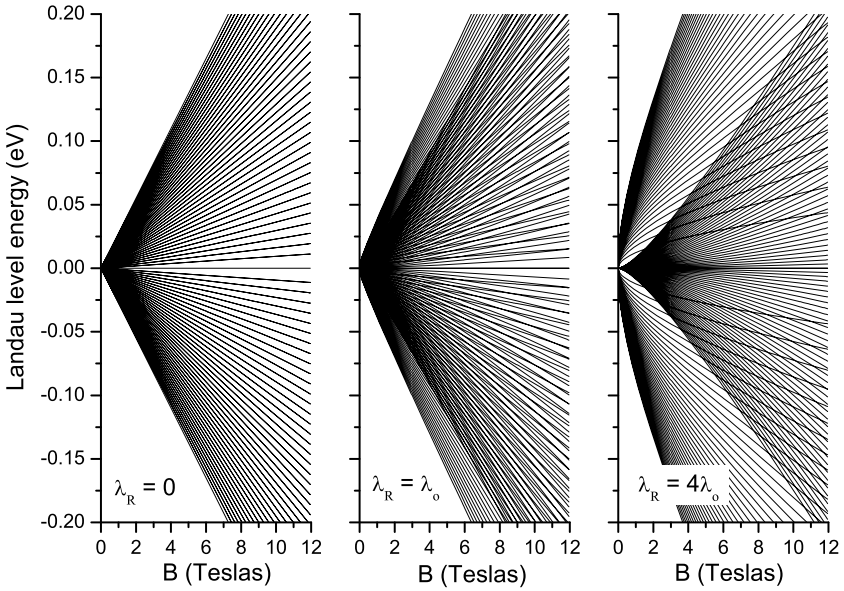

Figure 4. Spectrum of the LLs for BLG with Rashba-SOI within the effective low-energy theory. A rather unusual characteristic of the LLs is predicted to occur at large values of the Rashba-SOI strength.

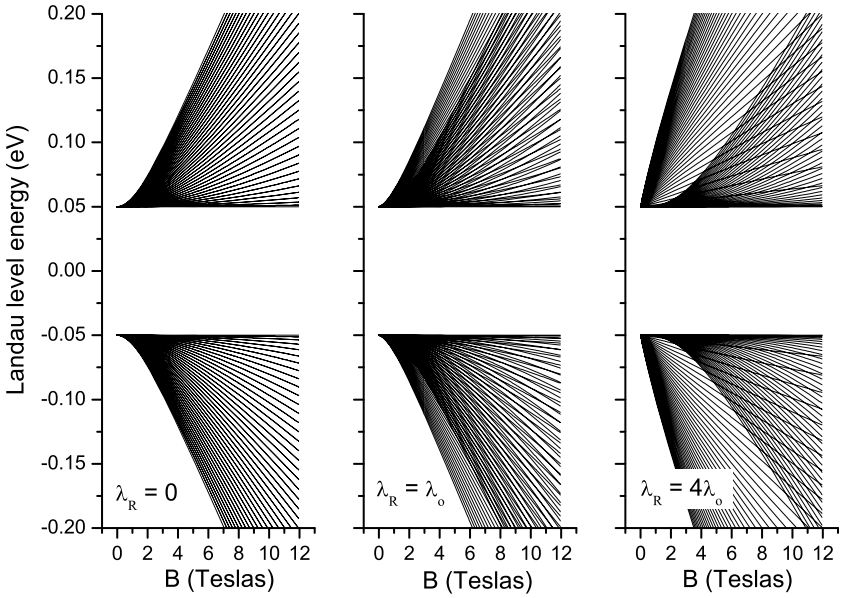

Figure 5. The presence of a bias voltage splits the fan diagram into two, opening a gap of $2U$ between the electron and hole LLs.

here to break the spin symmetry. When the Rashba-SOI is present, the spin degeneracy is lifted, inducing multiple crossings of the LLs at the Fermi energy, similarly to what occurs in semiconductor two-dimensional electron gases (2DEGs) with Rashba-SOI, and happens because for sizable λ_R strengths the LLs with high index and with spin chirality $s = +$ have

lower energies than those with spin chirality $s = -$ when the field is increased. This is basically an intermediate regime between those LLs discussed in sections 3.1(ii) and (iii). Note that for a relatively weak intensity of the Rashba parameter ($\lambda_R = \lambda_0$) the LLs behave roughly linearly with the field (figure 4(b)), no matter what the spin chirality.

However, for large values ($\lambda_R = 4\lambda_0$) a drastic and unusual change in the LL spectrum arises (figure 4(c)); the LLs with spin $\nu = +$ evolve as $B^{1/2}$ while those with $\nu = -$ develop a $B^{3/2}$ dependence as described in section 3.1(iii). Such a difference in the field dependence effectively squeezes the LLs with $\nu = -$ to lower energies when λ_R is increased, promoting multiple crossings between the LLs. This surprising result suggests a strong spin polarization of the LLs induced by a significant increase of the Rashba parameter.

The LLs for the biased $U \neq 0$ and without Rashba coupling case show instead parabolic behavior with B, and the fan diagram is split by a gap of $2U$ (figure 5(a)) as also described by equation (32). The linear behavior observed for $U = 0$ and $\lambda_R = \lambda_0$ of the LLs transforms as well to a B^2 dependence for $U \neq 0$, as predicted by equation (33). The presence of the Rashba-SOI manifests as well as crossings of the LLs as seen in figure 5(b). The behavior illustrated in figure 5(c) at relatively large λ_R is similar to that seen in figure 4(c), but with an open gap and with almost linear behavior with field for $\nu = +$, and a roughly cubic dependence on B for the $\nu = -$ LLs, see also equation (34). Such an asymmetric response at large Rashba-SOI in BLG contrasts radically with the linear behavior with field that occurs in single-layer graphene [37] in the same regime.

6. Summary

We have studied the problem of the influence of the Rashba-SOI on the band structure of biased and unbiased BLG. Using low-energy effective theory, we have derived a low-energy Hamiltonian for BLG in the presence of an external magnetic field and SOIs. Analytical formulae for the energy spectrum of a graphene bilayer with Rashba-SOI are obtained. We show that for a relatively weak Rashba coupling the spin degeneracy of the electron and hole bands is broken, inducing a k-linear spin splitting very similar to that found in semiconductor heterostructures. At intermediate strengths of the Rashba effect, the innermost bands interpolate from k-linear behavior at small momentum, to k-cubic dependence at high momentum. In contrast, the outermost bands seem to be well described by the cubic spectrum for all values of k. For large values of the Rashba coupling there is remarkable warping behavior of the spectrum near the Dirac point. Such behavior is unique in biased BLG. It is found that the bias-induced gap in BLG decreases when the Rashba is increased, showing behavior resembling a topological insulator transition phenomenon. These peculiar characteristics of the spectrum of BLG with Rashba-SOI may have important consequences for its electronic and spin-transport properties.

We also obtained an analytical expression for the LLs and spin polarization in biased BLG with the Rashba effect valid in the low bias regime. It is further predicted that unexpected asymmetric spin splitting and crossings of the LLs appear because of the interplay between the Rashba interaction and the bias voltage. These results suggest significant consequences for the Shubnikov–de Hass oscillations and magnetotransport in BLG as quantum and spin Hall effects, in the presence of sizable Rashba-SOI in the range of a few meVs.

Acknowledgments

FM is grateful to J Hausinger for useful discussions. This work was supported by Deutsche Forschungsgemeinschaft via GRK 1570 and by the Mexican grant Papiit-UNAM no. IN109911-3.

Appendix A. Derivation of the low-energy Hamiltonian

In this appendix, we derive the low-energy Hamiltonian for BLG in the presence of both intrinsic and Rashba-SOIs, as well as the Zeeman effect. The low-energy Hamiltonian is obtained via Löwdin partitioning, also known as van Vleck's perturbation theory in the context of atomic physics [43–45]. First, it is convenient to express the Hamiltonian H_k of equation (5) in the new spin-dependent atomic basis $|\tilde{\Psi}_K^\dagger\rangle = \{\psi_{A_{2\uparrow}}, \psi_{A_{2\downarrow}}, \psi_{B_{1\uparrow}}, \psi_{B_{1\downarrow}}, \psi_{A_{1\uparrow}}, \psi_{A_{1\downarrow}}, \psi_{B_{2\uparrow}}, \psi_{B_{2\downarrow}}\}$, leading to the 8×8 Hamiltonian

$$H_k = \begin{pmatrix} -U+\eta+\Delta & 0 & 0 & 0 & 0 & 0 & \gamma\pi & 0 \\ 0 & -U-\eta-\Delta & 0 & 0 & 0 & 0 & \mathrm{i}\lambda_R & \gamma\pi \\ 0 & 0 & U-\eta+\Delta & 0 & \gamma\pi^\dagger & -\mathrm{i}\lambda_R & 0 & 0 \\ 0 & 0 & 0 & U+\eta-\Delta & 0 & \gamma\pi^\dagger & 0 & 0 \\ 0 & 0 & \gamma\pi & 0 & U+\eta+\Delta & 0 & \gamma_1 & 0 \\ 0 & 0 & \mathrm{i}\lambda_R & \gamma\pi & 0 & U-\eta-\Delta & 0 & \gamma_1 \\ \gamma\pi^\dagger & -\mathrm{i}\lambda_R & 0 & 0 & \gamma_1 & 0 & -U-\eta+\Delta & 0 \\ 0 & \gamma\pi^\dagger & 0 & 0 & 0 & \gamma_1 & 0 & -U+\eta-\Delta \end{pmatrix}, \quad \text{(A.1)}$$

which can now be written as the sum $H_k = \mathcal{H}_0 + W$, with $\{U, \gamma_1, \Delta, \eta\} \in \mathcal{H}_0$ and $\{\lambda_R, \gamma\pi, \gamma\pi^\dagger\} \in W$ where

$$\mathcal{H}_0 = \begin{pmatrix} \mathcal{H}_+ & 0 \\ 0 & \mathcal{H}_- \end{pmatrix}, \quad \mathcal{H}_\pm = \begin{pmatrix} \mp U+\Delta+\eta & 0 & \gamma_1\,\delta_\pm & 0 \\ 0 & \mp U-\Delta-\eta & 0 & \gamma_1\,\delta_\pm \\ \gamma_1\,\delta_\pm & 0 & \pm U+\Delta-\eta & 0 \\ 0 & \gamma_1\,\delta_\pm & 0 & \pm U-\Delta-\eta \end{pmatrix}, \quad \text{(A.2)}$$

with $\delta_+ = 0$ and $\delta_- = 1$. On the other hand,

$$W = \begin{pmatrix} 0 & H_s \\ H_s & 0 \end{pmatrix} \quad \text{with } H_s = \begin{pmatrix} 0 & 0 & \gamma\pi & 0 \\ 0 & 0 & \mathrm{i}\lambda_R & \gamma\pi \\ \gamma\pi^\dagger & -\mathrm{i}\lambda_R & 0 & 0 \\ 0 & \gamma\pi^\dagger & 0 & 0 \end{pmatrix}. \quad \text{(A.3)}$$

Note that H_s is nothing but the single-layer graphene Hamiltonian with Rashba-SOI in the basis $\{\psi_{A_{2(1)\uparrow}}, \psi_{A_{2(1)\downarrow}}, \psi_{B_{1(2)\uparrow}}, \psi_{B_{1(2)\downarrow}}\}$.

BLG with Rashba-SOI, intrinsic-SOI and the Zeeman effect has (in general) eight non-degenerate levels. The levels are given by the eigenvalues of the Hamiltonian $\mathcal{H}_0$:

$$E_1^0 = -\Delta - \sqrt{\gamma_1^2 + (U+\eta)^2}, \quad \text{(A.4)}$$

$$E_2^0 = \Delta - \sqrt{\gamma_1^2 + (U-\eta)^2}, \quad \text{(A.5)}$$

$$E_3^0 = -U - \eta - \Delta, \quad \text{(A.6)}$$

$$E_4^0 = -U + \eta + \Delta, \quad \text{(A.7)}$$

$$E_5^0 = U - \eta + \Delta, \tag{A.8}$$

$$E_6^0 = U + \eta - \Delta, \tag{A.9}$$

$$E_7^0 = -\Delta + \sqrt{\gamma_1^2 + (U-\eta)^2}, \tag{A.10}$$

$$E_8^0 = \Delta + \sqrt{\gamma_1^2 + (U+\eta)^2}. \tag{A.11}$$

The eigenvectors $|\Psi_\mu\rangle$ of $\mathcal{H}_0$ (with $\mu = 1, 8$) can be written as column vectors of the matrix

$$\begin{pmatrix} 0 & 0 & 0 & 1 & 0 & 0 & 0 & 0 \\ 0 & 0 & 1 & 0 & 0 & 0 & 0 & 0 \\ 0 & 0 & 0 & 0 & 1 & 0 & 0 & 0 \\ 0 & 0 & 0 & 0 & 0 & 1 & 0 & 0 \\ 0 & -\mathcal{S}_+ & 0 & 0 & 0 & 0 & 0 & \mathcal{C}_+ \\ -\mathcal{S}_- & 0 & 0 & 0 & 0 & 0 & \mathcal{C}_- & 0 \\ 0 & \mathcal{C}_+ & 0 & 0 & 0 & 0 & 0 & \mathcal{S}_+ \\ \mathcal{C}_- & 0 & 0 & 0 & 0 & 0 & \mathcal{S}_- & 0 \end{pmatrix} \tag{A.12}$$

with $\mathcal{C}_\pm = \cos(\vartheta_\pm/2)$, $\mathcal{S}_\pm = \sin\left(\vartheta_\pm/2\right)$ and $\tan\vartheta_\pm = \gamma_1/(U \pm \eta)$. Because of the strength of the parameter γ_1, the energy levels of the subspace of high energy, $\mathcal{E}_{ia}^0 \in \left\{E_1^0, E_2^0, E_7^0, E_8^0\right\}$, and the energy levels of the subspace with low energy, $\mathcal{E}_{jb}^0 \in \left\{E_3^0, E_4^0, E_5^0, E_6^0\right\}$, are well separated from each other (i.e. $|\mathcal{E}_{ia}^0 - \mathcal{E}_{ja}^0| \sim |\mathcal{E}_{ib}^0 - \mathcal{E}_{jb}^0| \ll |\mathcal{E}_{ia}^0 - \mathcal{E}_{jb}^0| \sim |\gamma_1|$). The low-energy Hamiltonian for BLG can thus be obtained through the unitary transformation $\mathcal{H} = \mathrm{e}^{\mathrm{i}S} H_k \, \mathrm{e}^{-\mathrm{i}S}$, in which the S matrix elements are given by

$$S_{\mu\nu} = \frac{\mathrm{i}W_{\mu\nu}}{E_\nu^0 - E_\mu^0} + \mathrm{i}\sum_{\mu'} \frac{W_{\mu\mu'}W_{\mu'\nu}}{\left(E_\nu^0 - E_\mu^0\right)\left(E_\nu^0 - E_{\mu'}^0\right)} - \mathrm{i}\sum_{\nu'} \frac{W_{\mu\nu'}W_{\nu'\nu}}{\left(E_\nu^0 - E_\mu^0\right)\left(E_{\nu'}^0 - E_\nu^0\right)}$$

with $S_{\mu\nu} = \left(S_{\nu\mu}\right)^\dagger$ and $W_{\mu\nu} = \langle\Psi_\mu|W|\Psi_\nu\rangle$. The low-energy matrix elements of the effective Hamiltonian up to second order in $1/\gamma_1$ are determined by

$$\mathcal{H}_{\mu\mu'} = E_\mu^0\delta_{\mu\mu'} + W_{\mu\mu'} + \frac{1}{2}\sum_\nu W_{\mu\nu}W_{\nu\mu'}\left(\frac{1}{E_\mu^0 - E_\nu^0} + \frac{1}{E_{\mu'}^0 - E_\nu^0}\right) + \mathcal{O}(2),$$

with $\mathcal{H}_{\mu\nu} = \left(\mathcal{H}_{\nu\mu}\right)^\dagger$ and $\mu, \mu' \in \{3, 4, 5, 6\}$ and $\nu, \nu' \in= \{1, 2, 7, 8\}$. The effective Hamiltonian matrix elements read

$$\mathcal{H}_{33} = -U - \eta - \Delta + \frac{2(U+\eta+\Delta)\lambda_\mathrm{R}^2}{\gamma_1^2} + \frac{2\gamma^2 U}{\gamma_1^2}\pi^\dagger\pi,$$

$$\mathcal{H}_{34} = \frac{\mathrm{i}(2U+\eta+\Delta)\lambda_\mathrm{R}}{{\gamma_1}^2}\pi$$

$$\mathcal{H}_{35} = \frac{-2\mathrm{i}\,\lambda_\mathrm{R}\gamma}{\gamma_1^2}\pi^\dagger,$$

$$\mathcal{H}_{36} = -\frac{\gamma^2}{\gamma_1}\left(\pi^\dagger\right)^2,$$

$$\mathcal{H}_{44} = -U + \eta + \Delta + \frac{2U\gamma^2}{{\gamma_1}^2}\pi^\dagger\pi,$$
$$\mathcal{H}_{45} = H_{36},$$
$$\mathcal{H}_{46} = 0,$$
$$\mathcal{H}_{55} = U - \eta + \Delta - \frac{2(U-\eta-\Delta){\lambda_{\mathrm{R}}}^2}{{\gamma_1}^2} - \frac{2U\gamma^2}{{\gamma_1}^2}\pi\pi^\dagger,$$
$$\mathcal{H}_{56} = \frac{2\mathrm{i}\,\lambda_{\mathrm{R}}\gamma}{{\gamma_1}^2}(U+\Delta)\,\pi^\dagger,$$
$$\mathcal{H}_{66} = U + \eta - \Delta - \frac{2U\gamma^2}{{\gamma_1}^2}\pi\pi^\dagger.$$

These matrix elements form the desired 4×4 low-energy Hamiltonian for BLG

$$\mathcal{H} = \begin{pmatrix} \mathcal{H}_{33} & \mathcal{H}_{34} & \mathcal{H}_{35} & \mathcal{H}_{36} \\ \mathcal{H}_{34}^\dagger & \mathcal{H}_{44} & \mathcal{H}_{45} & \mathcal{H}_{46} \\ \mathcal{H}_{35}^\dagger & \mathcal{H}_{45}^\dagger & \mathcal{H}_{55} & \mathcal{H}_{56} \\ \mathcal{H}_{36}^\dagger & \mathcal{H}_{46}^\dagger & \mathcal{H}_{56}^\dagger & \mathcal{H}_{66} \end{pmatrix}, \tag{A.13}$$

which when written in terms of suitable Kronecker products leads to equation (10). Note that equation (A.13) was projected on the basis set $\{\psi_{A_{2\downarrow}}, \psi_{A_{2\uparrow}}, \psi_{B_{1\uparrow}}, \psi_{B_{1\downarrow}}\}$.

Energy dispersion. Consider vanishing intrinsic SOI and no magnetic field ($\eta = \Delta = 0$). To a good approximation, we can neglect the off-diagonal terms that go as $1/\gamma_1^2$ in the effective Hamiltonian. In such a case the eigenvalues of (A.13) are readily obtained:

$$E_{\lambda s}(k) = \frac{\lambda}{\sqrt{2}}\sqrt{U^2 + (U-\rho)^2 + \mathcal{A}k^2 + 2\mathcal{B}k^4 - s\sqrt{\Upsilon}}, \tag{A.14}$$

where λ indicates the electron (+) and hole (−) branches, whereas $s = \pm$ labels the spin state chirality, $\mathcal{A} = \Lambda - 4\tilde{\xi}\,U$, $\mathcal{B} = \tilde{\beta}^2 + \tilde{\xi}^2$, $\Lambda = \tilde{\alpha}^2 + 2\tilde{\xi}\rho$ and $\Upsilon = 4\alpha^2\tilde{\beta}^2k^6 + \left(\Lambda^2 + 4\rho^2\tilde{\beta}^2\right)k^4 - 2\rho\Lambda(2U-\rho)k^2 + \rho^2(2U-\rho)^2$, where we have introduced the parameters

$$\tilde{\alpha} = \frac{2\hbar\gamma\,\lambda_{\mathrm{R}}}{\gamma_1}, \quad \tilde{\beta} = \frac{\hbar^2\gamma^2}{\gamma_1}, \quad \rho = \frac{2U\lambda_{\mathrm{R}}}{{\gamma_1}^2}, \quad \tilde{\xi} = \frac{2U\hbar^2\gamma^2}{\gamma_1^2}. \tag{A.15}$$

In the limit $\rho \to 0$, equation (A.14) reduces to equation (14) with $\lambda = \mu$.

Appendix B. Eigenvalues of the low-energy Hamiltonian

By squaring the low-energy Hamiltonian (13), a straightforward diagonalizable system is obtained at zero magnetic field ($B = 0$):

$$\mathcal{H}_k^2 = \begin{pmatrix} (U-\xi k^2)^2 + \beta^2k^4 & -\mathrm{i}\alpha\beta\,k^2\,k_- & 0 & 0 \\ \mathrm{i}\alpha\beta\,k^2\,k_+ & (U-\xi k^2)^2 + \alpha^2k^2 + \beta^2k^4 & 0 & 0 \\ 0 & 0 & (U-\xi k^2)^2 + \alpha^2k^2 + \beta^2k^4 & -\mathrm{i}\alpha\beta\,k^2\,k_- \\ 0 & 0 & \mathrm{i}\alpha\beta\,k^2\,k_+ & (U-\xi k^2)^2 + \beta^2k^4 \end{pmatrix} \tag{B.1}$$

with $k_\pm = k_x \pm k_y$ and the eigensystem $\mathcal{H}_k^2|\chi\rangle = \varepsilon_k^2|\chi\rangle$ yields the eigenvalues

$$\varepsilon_{k,\pm}^2 = (U-\xi k^2)^2 + \tfrac{1}{2}k^2\left(\alpha^2 + 2\beta^2k^2 \pm \alpha\sqrt{\alpha^2 + 4\beta^2k^2}\right), \tag{B.2}$$

whereas its eigenvectors $|\chi_j\rangle$ arranged as column vectors form a unitary matrix,

$$\mathbb{U} = \begin{pmatrix} -\mathrm{i}\sin(\theta/2) & 0 & \mathrm{i}\cos(\theta/2) & 0 \\ \mathrm{e}^{\mathrm{i}\phi}\cos(\theta/2) & 0 & \mathrm{e}^{\mathrm{i}\phi}\sin(\theta/2) & 0 \\ 0 & -\mathrm{i}\cos(\theta/2) & 0 & \mathrm{i}\sin(\theta/2) \\ 0 & \mathrm{e}^{\mathrm{i}\phi}\sin(\theta/2) & 0 & \mathrm{e}^{\mathrm{i}\phi}\cos(\theta/2) \end{pmatrix}, \tag{B.3}$$

with $\tan\theta = 2\beta k/\alpha$, $\mathrm{e}^{\mathrm{i}\phi} = (k_x + \mathrm{i}k_y)/k$ and $\mathbb{U}^\dagger = \mathbb{U}^{-1}$. In the basis of the eigenvectors of $\mathcal{H}_k^2$, the 4×4 Hamiltonian $\mathcal{H}_k$ is conveniently transformed as follows:

$$\tilde{\mathcal{H}}_k = \mathbb{U}^\dagger \mathcal{H}_k \mathbb{U} = \begin{pmatrix} -U+\xi k^2 & r_+^* & 0 & s^* \\ r_+ & U-\xi k^2 & -s & 0 \\ 0 & -s^* & -U+\xi k^2 & r_-^* \\ s & 0 & r_- & U-\xi k^2 \end{pmatrix}, \tag{B.4}$$

and $|\tilde{\psi}_k\rangle = \mathbb{U}^{-1}|\psi_k\rangle$, where

$$\begin{aligned} r_\pm &= -\frac{1}{2}k\,\mathrm{e}^{2\mathrm{i}\phi}\left[2\beta k\sin\theta + \alpha(\cos\theta \mp 1)\right] \\ &= -\frac{1}{2}k\,\mathrm{e}^{2\mathrm{i}\phi}\left[\sqrt{\alpha^2+4\beta^2k^2} \pm \alpha\right] \end{aligned} \tag{B.5}$$

with

$$\sin\theta = \frac{2\beta k}{\sqrt{\alpha^2+4\beta^2k^2}}, \quad \cos\theta = \frac{\alpha}{\sqrt{\alpha^2+4\beta^2k^2}}, \tag{B.6}$$

whereas

$$s = -\frac{1}{2}k\,\mathrm{e}^{2\mathrm{i}\phi}[2\beta k\cos\theta - \alpha\sin\theta] = 0. \tag{B.7}$$

The eigenvalues of $\tilde{\mathcal{H}}_k$ are determined from $\varepsilon_{\mu s}(k) = \mu\sqrt{(U-\xi k^2)^2 + |r_s|^2}$, with $\mu = \pm$ for the electron/hole band and $s = \pm$ labeling the spin chirality state. Explicitly,

$$\varepsilon_{\mu s}(k) = \frac{\mu}{2}\sqrt{4\,(U-\xi k^2)^2 + k^2\left(\sqrt{\alpha^2+4k^2\beta^2} - s\,\alpha\right)^2}. \tag{B.8}$$

The eigenvectors of $\tilde{\mathcal{H}}_k$ are given by

$$|\tilde{\psi}_1\rangle = \frac{1}{\sqrt{1+(\chi_+^{(-)})^2}}\begin{pmatrix} \mathrm{i}\,\mathrm{e}^{-2\mathrm{i}\phi}\chi_+^{(-)} \\ 1 \\ 0 \\ 0 \end{pmatrix}, \quad |\tilde{\psi}_2\rangle = \frac{1}{\sqrt{1+(\chi_-^{(-)})^2}}\begin{pmatrix} 0 \\ 0 \\ \mathrm{i}\,\mathrm{e}^{-2\mathrm{i}\phi}\chi_-^{(-)} \\ 1 \end{pmatrix}, \tag{B.9}$$

$$|\tilde{\psi}_3\rangle = \frac{1}{\sqrt{1+(\chi_+^{(+)})^2}}\begin{pmatrix} \mathrm{i}\,\mathrm{e}^{-2\mathrm{i}\phi}\chi_+^{(+)} \\ 1 \\ 0 \\ 0 \end{pmatrix}, \quad |\tilde{\psi}_4\rangle = \frac{1}{\sqrt{1+(\chi_-^{(+)})^2}}\begin{pmatrix} 0 \\ 0 \\ \mathrm{i}\,\mathrm{e}^{-2\mathrm{i}\phi}\chi_-^{(+)} \\ 1 \end{pmatrix}. \tag{B.10}$$

The eigenvectors of $\mathcal{H}_k$ are finally given by $|\psi_k\rangle = \mathbb{U}|\tilde{\psi}_k\rangle$ leading to equations (17) and (18) with $\chi_s^{(\mu)}$ as given by equation (19).

Appendix C. LLs in BLG with Rashba coupling

Here we outline the derivation of the LLs in biased BLG with Rashba-SOI. We follow the same approach used in appendix B. Squaring the Hamiltonian (28) gives the block-diagonal matrix

$$\mathcal{H}_n^2 = \begin{pmatrix} U^2+(n-1)n\omega^2 & -\mathrm{i}n\sqrt{n-1}\,\Gamma\omega & 0 & 0 \\ \mathrm{i}n\sqrt{n-1}\,\Gamma\omega & U^2+n\left(\Gamma^2+(n+1)\,\omega^2\right) & 0 & 0 \\ 0 & 0 & U^2+n\left(\Gamma^2+(n-1)\,\omega^2\right) & -\mathrm{i}n\sqrt{n+1}\,\Gamma\,\omega \\ 0 & 0 & \mathrm{i}n\sqrt{n+1}\,\Gamma\omega & U^2+n(n+1)\,\omega^2 \end{pmatrix}, \tag{C.1}$$

the eigensystem $\mathcal{H}_n^2|\varphi_n\rangle = \varepsilon_n^2|\varphi_n\rangle$ leads to the eigenvalues

$$\varepsilon_{n,\pm}^2 = \frac{1}{2}\left(2\,U^2+2n^2\omega^2+n\Gamma^2 \pm n\sqrt{4\omega^4+4n\omega^2\Gamma^2+\Gamma^4}\right), \tag{C.2}$$

and its corresponding eigenvectors $|\varphi_{nj}\rangle$ written as column vectors form the matrix

$$\mathbb{V} = \begin{pmatrix} 0 & \mathrm{i}\cos\vartheta_{n+} & 0 & -\mathrm{i}\sin\vartheta_{n+} \\ 0 & \sin\vartheta_{n+} & 0 & \cos\vartheta_{n+} \\ \mathrm{i}\cos\vartheta_{n-} & 0 & -\mathrm{i}\sin\vartheta_{n-} & 0 \\ \sin\vartheta_{n-} & 0 & \cos\vartheta_{n-} & 0 \end{pmatrix}, \quad \tan(\vartheta_{n\pm}) = \frac{2\sqrt{n\mp1}\,\omega\,\Gamma}{2\,\omega^2\pm\Gamma^2} \tag{C.3}$$

and $\mathbb{V}^\dagger\mathbb{V}=1$. In the basis of the eigenvectors of $\mathcal{H}_n^2$, the 4×4 Hamiltonian $\mathcal{H}_n$ in equation (28) is now transformed as follows:

$$\tilde{\mathcal{H}}_n = \mathbb{V}^\dagger\mathcal{H}_n\mathbb{V} = \begin{pmatrix} \mathcal{U} & Q_{n-} & 0 & u_n \\ Q_{n-} & -\mathcal{U} & v_n & 0 \\ 0 & v_n & \mathcal{U} & Q_{n+} \\ u_n & 0 & Q_{n+} & -\mathcal{U} \end{pmatrix} \quad \text{and} \quad |\tilde{\phi}_n\rangle = \mathbb{V}^{-1}|\phi_n\rangle, \tag{C.4}$$

where

$$\begin{aligned} Q_{n\pm} &= -\omega\left(\sqrt{n(n\pm1)}\cos\vartheta_+\cos\vartheta_- + \sqrt{n(n\mp1)}\sin\vartheta_+\sin\vartheta_-\right) \mp \sqrt{n}\,\Gamma\cos\vartheta_\pm\sin\vartheta_\mp \\ &= -4\omega^2\Gamma\frac{\sqrt{n(n^2-1)\,\mathcal{N}_n}}{\sqrt{\mathcal{D}_{1\mp}\mathcal{D}_{2\pm}}}, \quad n>1, \end{aligned} \tag{C.5}$$

where we have used the useful relationships:

$$\cos\vartheta_{n+} = \frac{2\omega^2+\Gamma^2+\sqrt{\mathcal{N}_n}}{\sqrt{\mathcal{D}_{1+}}} = \frac{2\sqrt{n-1}\,\omega\,\Gamma}{\sqrt{\mathcal{D}_{1-}}}, \tag{C.6}$$

$$\sin\vartheta_{n+} = \frac{2\sqrt{n-1}\,\omega\,\Gamma}{\sqrt{\mathcal{D}_{1+}}} = -\frac{2\beta^2+\Gamma^2-\sqrt{\mathcal{N}_n}}{\sqrt{\mathcal{D}_{1-}}}, \tag{C.7}$$

$$\cos\vartheta_{n-} = \frac{2\omega^2-\Gamma^2+\sqrt{\mathcal{N}_n}}{\sqrt{\mathcal{D}_{2+}}} = \frac{2\sqrt{n+1}\,\omega\,\Gamma}{\sqrt{\mathcal{D}_{2-}}}, \tag{C.8}$$

$$\sin\vartheta_{n-} = \frac{2\sqrt{n+1}\,\omega\,\Gamma}{\sqrt{\mathcal{D}_{2+}}} = -\frac{2\beta^2-\Gamma^2-\sqrt{\mathcal{N}_n}}{\sqrt{\mathcal{D}_{2-}}} \tag{C.9}$$

with the definitions of the parameters

$$\mathcal{N}_n = 4\,\omega^2(\omega^2+n\Gamma^2)+\Gamma^4, \tag{C.10}$$

$$\mathcal{D}_{1\pm} = (4n-1)\omega^2\Gamma^2 + \left(2\omega^2 + \Gamma^2 \pm \sqrt{\mathcal{N}_n}\right)^2, \tag{C.11}$$

$$\mathcal{D}_{2\pm} = (4n+1)\omega^2\Gamma^2 + \left(2\omega^2 - \Gamma^2 \pm \sqrt{\mathcal{N}_n}\right)^2. \tag{C.12}$$

Note that

$$u_n = -\omega\left(\sqrt{n(n+1)}\cos\vartheta_{n+}\sin\vartheta_{n-} - \sqrt{n(n-1)}\sin\vartheta_{n+}\cos\vartheta_{n-}\right) - \sqrt{n}\,\Gamma\cos\vartheta_{n+}\cos\vartheta_{n-} = 0, \tag{C.13}$$

$$v_n = -\omega\left(\sqrt{n(n+1)}\cos\vartheta_{n-}\sin\vartheta_{n+} - \sqrt{n(n-1)}\sin\vartheta_{n-}\cos\vartheta_{n+}\right) + \sqrt{n}\,\Gamma\sin\vartheta_{n+}\sin\vartheta_{n-} = 0, \tag{C.14}$$

The LLs of BLG with Rashba-SOI are thus determined by the eigenvalues of $\tilde{\mathcal{H}}_n$, which yields

$$\varepsilon_{n,\mu\nu} = \mu\sqrt{U^2 + |Q_{n\nu}|^2}, \tag{C.15}$$

for $n \geqslant 2$, with n being the LL index with $\nu = \pm$ (plus/minus) state of the $\mu = \pm$ electron (hole) band. Using equations (C.5) along with (C.10)–(C.12), formula (2) readily follows. The eigenvectors of $\tilde{\mathcal{H}}_n$ are given by

$$|\tilde{\phi}_{n1}\rangle = \begin{pmatrix} 0 \\ \cos\eta_- \\ \sin\eta_- \\ 0 \end{pmatrix}, \quad |\tilde{\phi}_{n2}\rangle = \begin{pmatrix} \cos\phi_- \\ \sin\phi_- \\ 0 \\ 0 \end{pmatrix}, \quad |\tilde{\phi}_{n3}\rangle = \begin{pmatrix} 0 \\ -\cos\eta_+ \\ \sin\eta_+ \\ 0 \end{pmatrix}, \quad |\tilde{\phi}_{n4}\rangle = \begin{pmatrix} -\cos\phi_+ \\ \sin\phi_+ \\ 0 \\ 0 \end{pmatrix}, \tag{C.16}$$

where the angles $\eta_\pm$ and $\phi_\pm$ satisfy

$$\tan\eta_\pm = \frac{1}{|P_\pm|} = \frac{|Q_{n+}|}{\left|U \pm \sqrt{U^2 + Q_{n+}^2}\right|} \quad \text{and} \quad \tan\phi_\pm = \frac{1}{|M_\pm|} = \frac{|Q_{n-}|}{\left|U \pm \sqrt{U^2 + Q_{n-}^2}\right|}, \tag{C.17}$$

with $M_-M_+ = P_+P_- = -1$. The eigenvectors of $\mathcal{H}_n$ are thus given by $|\phi_{nj}\rangle = \mathbb{V}|\tilde{\phi}_{nj}\rangle$, and consequently, the eigenvectors of $\hat{H}_n$ are finally determined by $|\psi_n\rangle = (\phi_{nj}^{(1)}\xi_{n-2},\, \phi_{nj}^{(2)}\xi_{n-1},\, \phi_{nj}^{(3)}\xi_n,\, \phi_{nj}^{(4)}\xi_{n+1})^T$. The normalized eigenvectors for the states $(\pm)$ of the nth LL of a given electron (hole) band μ are thus explicitly specified by

$$|\psi_{n\mu}^{(+)}\rangle = \begin{pmatrix} -\mathrm{i}\sin\vartheta_{n+}\sin\eta_\mu\,\xi_{n-2} \\ \cos\vartheta_{n+}\sin\eta_\mu\,\xi_{n-1} \\ \mathrm{i}\sin\vartheta_{n-}\cos\eta_\mu\,\xi_n \\ -\cos\vartheta_{n-}\cos\eta_\mu\,\xi_{n+1} \end{pmatrix}, \qquad |\psi_{n\mu}^{(-)}\rangle = \begin{pmatrix} \mathrm{i}\cos\vartheta_{n+}\sin\eta_\mu\,\xi_{n-2} \\ \sin\vartheta_{n+}\sin\eta_\mu\,\xi_{n-1} \\ -\mathrm{i}\cos\vartheta_{n-}\cos\varphi_\mu\,\xi_n \\ -\sin\vartheta_{n-}\cos\varphi_\mu\,\xi_{n+1} \end{pmatrix}, \tag{C.18}$$

From equations (C.18) and the orthogonality of the oscillator wave functions ξ_n, it follows that the components in the plane of BLG of both the valley and spin polarization, vanish identically for all LLs, $\langle\tau_x^{(n)}\rangle_{\mu\nu} = \langle\tau_y^{(n)}\rangle_{\mu\nu} = 0$ and $\langle S_x^{(n)}\rangle_{\mu\nu} = \langle S_x^{(n)}\rangle_{\mu\nu} = 0$. The valley polarization in the perpendicular direction (along the z-axis) reads

$$\langle\tau_z^{(\nu)}\rangle_{n,\mu} = \begin{cases} -\cos(2\eta_\mu)\,, & \text{for } \nu = +, \\ \sin^2\eta_\mu - \cos^2\varphi_\mu\,, & \text{for } \nu = -. \end{cases} \tag{C.19}$$

Note that it is k-independent and that in the limit case of zero bias voltage ($U = 0$) results in $\eta_\pm = \phi_\pm = \frac{\pi}{4}$, and hence a zero valley polarization. The zth component of the spin polarization gives, on the other hand,

$$\langle S_z^{(\nu)} \rangle_{n,\mu} = \begin{cases} -\cos\vartheta_{n-}\cos^2\eta_\mu - \cos\vartheta_{n+}\sin^2\eta_\mu, & \nu = +, \\ \cos\vartheta_{n-}\cos^2\varphi_\mu + \cos\vartheta_{n+}\sin^2\eta_\mu, & \nu = -, \end{cases} \tag{C.20}$$

which in the absence of bias voltage simplifies to equation (35).

References

[1] Castro Neto A H, Guinea F, Peres N M R, Novoselov K S and Geim A K 2009 *Rev. Mod. Phys.* **81** 109
[2] Castro E V, Novoselov K S, Morozov S V, Peres N M R, Lopes dos Santos J M B, Nilsson J, Guinea F, Geim A K and Castro Neto A H 2010 *J. Phys.: Condens. Matter* **22** 175503
[3] Das Sarma S, Adam S, Hwang E H and Rossi E 2011 *Rev. Mod. Phys.* **83** 407–70
[4] Abergela D S L, Apalkov V, Berashevich J, Ziegler K and Chakraborty T 2010 *Adv. Phys.* **59** 261
[5] Peres N M R 2010 *Rev. Mod. Phys.* **82** 2673
[6] Haldane F D M 1988 *Phys. Rev. Lett.* **61** 2015
[7] Novoselov K S, McCann E, Mozorov S V, Fal'ko V I, Katsnelson M I, Zeitler U, Maan J C, Boebinger G S, Kim P and Geim A K 2007 *Science* **315** 1379
[8] Du X, Skachko I, Duerr F, Luican A and Andrei E Y 2009 *Nature* **462** 192
[9] Bolotin K I, Ghahari F, Shulman M D, Stormer H L and Kim P 2009 *Nature* **462** 196
[10] Nakamura M, Hirasawa L and Imura K I 2008 *Phys. Rev.* B **78** 033403
[11] Koshino M and McCann E 2010 *Phys. Rev.* B **81** 115315
[12] Pereira M, Peeters F M and Vasilopoulus P 2007 *Phys. Rev.* B **76** 115419
[13] McCann E and Fal'ko V 2006 *Phys. Rev. Lett.* **96** 086805
[14] Abergel D S L and Fal'ko V I 2007 *Phys. Rev.* B **75** 155430
[15] McCann E and Koshino M 2012 arXiv:1205.6953v1
[16] Neugebauer P, Orlita M, Faugeras C, Barra A-L and Potemski M 2009 *Phys. Rev. Lett.* **103** 136403
[17] Henriksen E A, Jiang Z, Tung L-C, Schwartz M E, Takita M, Wang Y-J, Kim P and Stormer H L 2008 *Phys. Rev. Lett.* **100** 087403
[18] Henriksen E A, Cadden-Zimansky P, Jiang Z, Li Z Q, Tung L-C, Schwartz M E, Takita M, Wang Y-J, Kim P and Stormer H L 2010 *Phys. Rev. Lett.* **104** 067404
[19] Faugeras C, Amado M, Kossacki P, Orlita M, Kühne M, Nicolet A A L, Latyshev Y I and Potemski M 2011 *Phys. Rev. Lett.* **107** 036807
[20] Zutic I, Fabian J and Das Sarma S 2004 *Rev. Mod. Phys.* **76** 323
[21] Yao Y, Ye F, Qi X-L, Zhang S-C and Fang Z 2007 *Phys. Rev.* B **75** 041401
[22] Min H, Hill J E, Sinitsyn N A, Sahu B R, Kleinman L and MacDonald A H 2006 *Phys. Rev.* B **74** 165310
[23] Huertas-Hernando D, Guinea F and Brataas A 2006 *Phys. Rev.* B **74** 155426
[24] Boettger J C and Trickey S B 2007 *Phys. Rev.* B **75** 121402
[25] Gmitra M, Konschuh S, Ertler C, Ambrosch-Draxl C and Fabian J 2009 *Phys. Rev.* B **80** 235431
[26] Konschuh S, Gmitra M and Fabian J 2010 *Phys. Rev.* B **82** 245412
[27] Konschuh S, Gmitra M, Kochan D and Fabian J 2012 *Phys. Rev.* B **85** 115423
[28] Varykhalov A, Sanchez-Barriga J, Shikin A M, Biswas C, Vescovo E, Rybkin A, Marchenko D and Rader O 2008 *Phys. Rev. Lett.* **101** 157601
[29] Castro Neto A H and Guinea F 2009 *Phys. Rev. Lett.* **103** 026804
[30] Weeks C, Hu J, Alicea J, Franz M and Wu R 2011 *Phys. Rev. X* **1** 021001
[31] Abdelouahed S, Ernst A, Henk J, Maznichenko I V and Mertig I 2010 *Phys. Rev.* B **82** 125424
[32] Yang T-Y *et al* 2012 *Phys. Rev. Lett.* **107** 047206
[33] Tombros N, Józsa C, Popinciuc M, Jonkman H T and van Wees B J 2007 *Nature* **448** 571

[34] Józsa C, Maassen T, Popinciuc M, Zomer P J, Veligura A, Jonkman H T and van Wees B J 2009 *Phys. Rev.* B **80** 241403
[35] Diez M and Burkard G 2012 arXiv:1202.2067v1
[36] Dedkov Y S, Fonin M, Rüdiger U and Laubschat C 2008 *Phys. Rev. Lett.* **100** 107602
[37] Rashba E I 2009 *Phys. Rev.* B **79** 161409
[38] Zarea M and Sandler N 2009 *Phys. Rev.* B **79** 165442
[39] van Gelderen R and Morais Smith C 2010 *Phys. Rev.* B **81** 125435
[40] De Martino A, Hütten A and Egger R 2011 *Phys. Rev.* B **88** 155420
[41] Kusmenko A B, Crassee I, van der Marel D, Blake P and Novoselov K S 2009 *Phys. Rev.* B **80** 165406
[42] Guinea F 2010 *New J. Phys.* **12** 083063
[43] van Vleck J H 1929 *Phys. Rev.* **33** 427
[44] Cohen-Tannoudji C, Dupont-Roc J and Grynberg G 2004 *Atom–Photon Interactions: Basic Processes and Applications* (New York: Wiley VCH)
[45] Zhang L M, Fogler M M and Arovas D P 2011 *Phys. Rev.* B **84** 075451
[46] Stauber T and Schliemann J 2009 *New J. Phys.* **11** 115003